Rare Met. (2023) 42(5):1732–1742
https://doi.org/10.1007/s12598-018-1119-6

RARE METALS
www.editorialmanager.com/rmet

Microstructural evolution and mechanical behavior of in situ synthesized $MgAl_2O_4$ whiskers reinforced 6061 Al alloy composite after hot extrusion and annealing

Geng Hao, Chun-Sheng Shi*, Nai-Qin Zhao, En-Zuo Liu, Chun-Nian He, Fang He, Li-Ying Ma

Received: 17 August 2017 / Revised: 23 November 2017 / Accepted: 3 July 2018 / Published online: 4 September 2018

Abstract In situ synthesized $MgAl_2O_4$ whiskers reinforced 6061 Al alloy composites were fabricated by a powder metallurgy method. Nano-sized $MgAl_2O_4$ spinel whiskers distributed uniformly in 6061 Al alloy matrix without any interfacial product and laid along the extrusion direction after hot extrusion. As-extruded composite samples were annealed at 530, 580, 600 and 630 °C for 1 h and examined by electron backscattered diffraction to investigate the recrystallization behavior of obtained composites. Microstructure and texture evolution was investigated, and it is found that the recrystallization process is inhibited by whiskers because of Zener pinning. Slender fibrous grains remain until 630 °C, and deformation textures still exist even in specimen annealed at 630 °C. Hardness and tensile tests show that the completely recrystallized sample has an ultimate tensile strength of 218 MPa and a hardness of HV 52 compared with 283 MPa and HV 69 of the unannealed sample. Mechanical properties of the annealed samples decline slightly with annealing temperature increasing up to 600 °C.

G. Hao, C.-S. Shi*, N.-Q. Zhao, E.-Z. Liu, C.-N. He, F. He, L.-Y. Ma
School of Materials Science and Engineering, Tianjin University, Tianjin 300350, China
e-mail: csshi@tju.edu.cn

G. Hao, C.-S. Shi, N.-Q. Zhao, E.-Z. Liu, C.-N. He, F. He, L.-Y. Ma
Tianjin Key Laboratory of Composite and Functional Materials, Tianjin University, Tianjin 300350, China

N.-Q. Zhao, E.-Z. Liu, C.-N. He
Collaborative Innovation Centre of Chemical Science and Engineering, Tianjin 300072, China

Keywords Composite; In situ synthesized whiskers; Recrystallization; Microstructure; Texture

1 Introduction

Discontinuously reinforced aluminum matrix composites (AMCs) have drawn considerable attention in many advanced applications in automotive, transportation and aerospace industries [1–3] due to their excellent mechanical and physical properties such as low density, high specific strength, good wear and corrosion resistance and good thermal stability [4–10].

The mechanical performance of AMCs is significantly influenced by the interfacial bonding and the distribution of reinforcement. Compared with the ex situ fabrication, an in situ method effectively avoids these problems [4–8, 11, 12]. The reinforcements synthesized by the in situ method usually have a very strong bonding with the matrix, and their distribution is homogeneous, resulting in improvement in the mechanical properties.

The mechanical properties of the deformed composites can be easily influenced by annealing [13, 14]. Both microstructure and texture evolve during the recrystallization annealing process. Elongated deformed grains tend to become equiaxed and deformation textures tend to transform into recrystallization textures, resulting in the decrease in strength. So if the recrystallization phenomenon of composites was retarded, the composites would present good mechanical properties after annealing, giving a promising application at elevated temperatures.

The deformation textures of aluminum alloys (fcc metal) mainly lie on α-fiber and β-fiber. Along α-fiber, the typical texture components are Goss orientation {011} <100>, brass orientation {011} <211>, and those along β-fiber are

S orientation {123} <634>, R orientation {124} <211> and cooper orientation {112} <111> [15]. While after annealing, cube orientation {001} <100> is usually found to be the dominant recrystallization texture [16]. And it is commonly understood that a noticeable Goss orientation {011} <100> in recrystallization texture can result in poor formability; on the contrary, a weak cube orientation significantly increases the limiting dome height [13].

However, the contribution of secondary phase still needs much discussion [17], since the secondary phase has crucial influence on the deformation and recrystallization process. It is now mainly agreed that the effects of large second-phase particles and small particles are quite different. Large second-phase particles (larger than 1 μm) provide ideal nucleation sites in the deformation zone for recrystallization, i.e., particle stimulated nucleation (PSN) [17]. And the small dispersion particles have strong Zener drag to pin the grain boundaries, sub-grain boundaries and dislocations, so the migration of them is prevented. Then recrystallization is inhibited.

Many studies about deformation textures or recrystallization textures of aluminum alloys and aluminum alloy matrix composites have been carried out [13–16, 18–26]. Deng et al. [16] investigated the texture of cold-rolled and recrystallized Al–Zn–Mg–Sc–Zr alloys and the nucleation mechanism of the recrystallization. Deng et al. [15] found nanoscale $MgZn_2$ particles yielded during thermomechanical processing can reduce the recrystallization content of Al–Zn–Mg–Cu alloy plate due to that the particles inhibit the migration of dislocations and grain boundaries. Jiang et al. [22] compared the extrusion textures of 6061/SiC_p composites and those of pure Al and 6061 alloy and found three moderate strong extrusion texture components close to the typical β-fiber in deformed fcc metals. Furthermore, Zhang et al. [27] found that both deformation texture components and recrystallization texture components of the obtained SiC_w/Al composite were weaker than those of pure aluminum.

In this work, the $MgAl_2O_4$ whiskers reinforced 6061 Al alloy composites were fabricated using an in situ method, and microstructure and texture of both the extruded samples and annealed samples were studied to investigate the evolution of microstructure and texture of composites during annealing.

2 Experimental

6061 Al powders with an average diameter of 36 μm, Mg powders with an average diameter of 10 μm and boric acid were used as the raw materials to fabricate the $MgAl_2O_4$ whiskers reinforced 6061 Al alloy composites. These powders were mixed in a mass ratio of 15:2:3, and 1 wt% stearic acid was also added as the process control agent to prevent excessive cold welding of the powders in the subsequent ball milling pretreatment. Then a ball milling pretreatment was carried out in a stainless steel chamber of 250 ml for 4 h with a ball-to-powder weight ratio of 10:1 at a speed of 400 r·min^{-1}. The obtained mixture was compacted into a bulk with 20 mm in diameter under a pressure of 600 MPa, and the bulk was sintered at 650 °C for 1 h in a tubular furnace with argon atmosphere protection to in situ generate $MgAl_2O_4$ whiskers. Afterward, the bulk was heated at 540 °C for 1 h and immediately hot-extruded in a steel mold with an extrusion ratio of 16:1. Finally, the rod samples were annealed at 530, 580, 600 and 630 °C for 1 h separately in a resistance furnace to further estimate the stability of microstructure at high temperatures.

X-ray diffraction (XRD) was carried out on a Bruker D8 advance diffractometer with Cu Kα radiation to identify the phase components. Scanning electron microscope (SEM, Hitachi S4800) was used to observe the microstructure of whiskers and the fracture surfaces of tensile test specimens. And high-resolution transmission electron microscope (HRTEM, JEM-2100F) was used to characterize the microstructure and interface of whiskers and the matrix in detail. To analyze the microstructure and texture of deformed and annealed composite specimens, electron backscattered diffraction (EBSD) was employed. The specimens were first ion polished and then examined by scanning electron microscope (SEM, FEI Quantan 650F) equipped with EBSD detector (Oxford HKL Nordlys). Electron energy loss spectrum (EELS) chemical analysis was carried out using aberration-corrected transmission electron microscope (TEM, FEI Titan Cubed Themis G2 300) and Enfinium ER Model 977 EELS spectrometer to determine whether the whiskers contained B element.

The hardness was evaluated on an MH-6 Vickers hardness device under loading weight of 200 g for 5 s from the average value of 8 measurements. And tensile tests of the composites were performed on an M350-20KN universal testing machine under 1 mm·min^{-1} monotonic loading at room temperature.

3 Results and discussion

3.1 In situ synthesis of whiskers/6061 Al composites

The 6061 Al powder, Mg powder and boric acid were mixed and sintered, and the reactions among the raw materials can be inferred as follows [5–8, 28]:

$$4H_3BO_3\,(\text{solid}) \rightarrow 2B_2O_3\,(\text{solid}) + 6H_2O\,(\text{gas}) \quad (1)$$

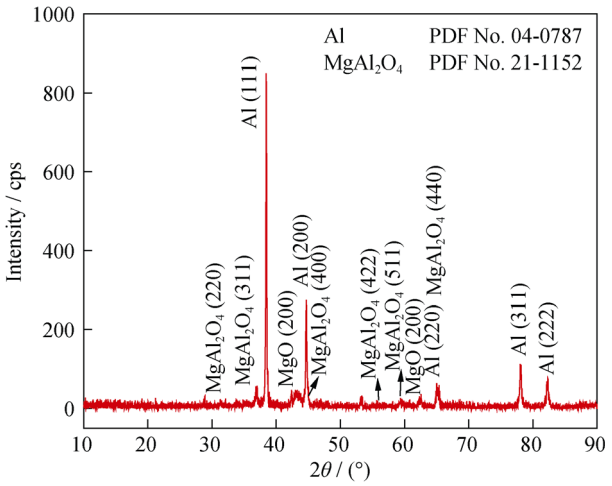

Fig. 1 XRD pattern of specimen after sintering at 650 °C for 1 h, showing existence of Al and $MgAl_2O_4$ spinel phases

$$B_2O_3\ (\text{solid}) \rightarrow B_2O_3\ (\text{liquid}) \quad (2)$$

$$4H_3BO_3\ (\text{solid}) + 6Al + 3Mg \rightarrow 3MgAl_2O_4 + 4B + 6H_2 \quad (3)$$

$$4B_2O_3\ (\text{liquid}) + 6Al + 3Mg \rightarrow 3MgAl_2O_4 + 8B \quad (4)$$

$$Mg + 2B \rightarrow MgB_2 \quad (5)$$

Figure 1 shows XRD pattern of as-sintered specimen. The peaks at 36°, 44° and 65° can be assigned to $MgAl_2O_4$ spinel, proving that the $MgAl_2O_4$ spinel was in situ synthesized successfully during the sintering process. Al is also recognized by XRD pattern (peaks at 38°, 44° and 78°), and the peaks are much stronger than that of $MgAl_2O_4$ spinel because of the high content of matrix in the obtained composites. However, MgB_2 is not detected by XRD due to its low content. To verify the morphology of the spinel phase, the specimen was eroded by HCl, and then the remnant was examined by XRD and observed by SEM. The SEM observation shown in Fig. 2 confirms the existence of whiskers, and the corresponding XRD pattern recognizes the whisker as $MgAl_2O_4$ spinel. So the $MgAl_2O_4$ spinel whiskers were successfully generated in the 6061 Al alloy matrix.

The obtained composites were examined by SEM and TEM to further characterize the whiskers. From SEM images shown in Fig. 3a, b, it is found that the diameter of the whiskers ranges from 30 to 100 nm with the aspect ratio ranging from 10 to 30. The whiskers uniformly distribute in the matrix without obvious agglomeration, and the most of the whiskers lay along extrusion direction (ED) due to the high stress during hot extrusion. The orientation of whiskers can significantly improve the tensile strength along the extrusion direction. However, it is unexpected that a small part of whiskers is broken during hot extrusion. SEM images (Fig. 3c, d) show a smooth and clean interface without interfacial products or precipitated phase between $MgAl_2O_4$ whisker and 6061 Al alloy matrix, reflecting the strong bonding of whisker and matrix. Figure 3d shows well crystallization of $MgAl_2O_4$ whisker that is elongated in the {220} direction. Besides the $MgAl_2O_4$ spinel whiskers, MgB_2, which was undetected by XRD due to its small amount in the obtained composites, is also found as whiskers by TEM (Fig. 3e). SAED pattern in the inset can be assigned to MgB_2 whiskers (Fig. 3e). EELS pattern shows B-enriched region (Region A) on a MgB_2 whisker and B-free region (Region B) on its adjacent whisker, indicating that both MgB_2 whisker and $MgAl_2O_4$ spinel whisker exist in the composites (Fig. 3f).

3.2 Microstructure of composites

Hot extrusion is an effective method to improve the compactness of powder metallurgy products and the strength of composites. Generally, most grains of hot-extruded samples are elongated along the extrusion direction (ED), and some grains may show equiaxed because of dynamic

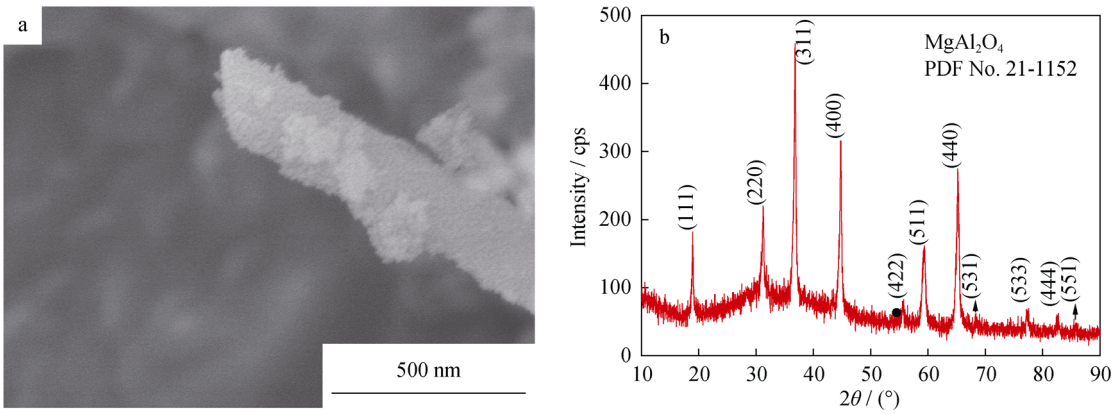

Fig. 2 **a** SEM image of remnant of composite after removal of matrix by HCl erosion and **b** corresponding XRD pattern showing remnant spinel $MgAl_2O_4$

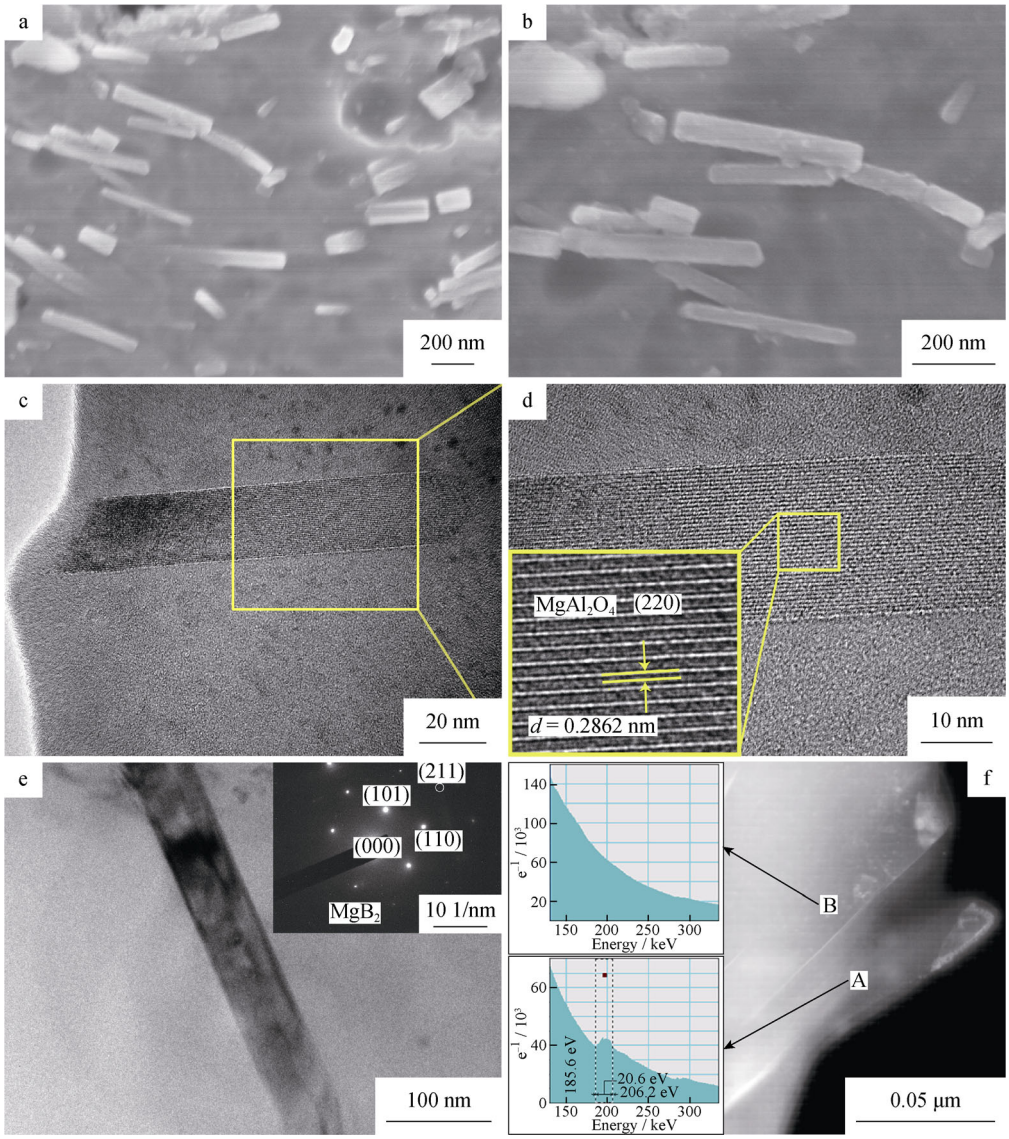

Fig. 3 **a**, **b** SEM images of whiskers in Al matrix after hot extrusion at 540 °C with an extrusion ratio of 16:1; **c**, **d** TEM images of $MgAl_2O_4$ spinel whiskers [inset **d** showing lattice planes of (220)]; **e** TEM image of MgB_2 whisker; **f** EELS patterns determining presence of B element in Region A and the absence of B element in Region B

recrystallization. The deformed grains are sensitive to temperature. When annealed at high temperatures, the deformed grains tend to recrystallize, resulting in equiaxed coarse grains. Secondary phase significantly influences the recrystallization, either promotes or inhibits recrystallization, depending on the size of secondary phase. In this work, the obtained $MgAl_2O_4$ whiskers reinforced 6061 Al alloys composites were annealed at 530, 580, 600 and 630 °C for 1 h separately to investigate the effect of whiskers on the annealing process. In addition, as-sintered and as-extruded specimens were also investigated for comparison.

Figure 4 shows microstructures of as-sintered specimen and as-extruded specimen. The grains of as-sintered specimen are equiaxed, with an average diameter of 30 μm. After hot extrusion, the deformed grains show slender fibrous elongated along ED. However, a very small amount of fine equiaxed grains are detected, suggesting that dynamic recrystallization partially occurs due to the high temperature and large extrusion ratio of the hot extrusion process [22]. During dynamic recrystallization, the grains nucleate but do not grow coarse, resulting in the grain refinement. And it is worth mentioning that the grains of as-sintered specimen are randomly oriented (Fig. 4a) while those of as-extruded specimen tend to have some preferred crystallographic orientation (Fig. 4b).

The grains and grain boundaries of as-extruded and annealed specimens are shown in Fig. 5. Low-angle grain

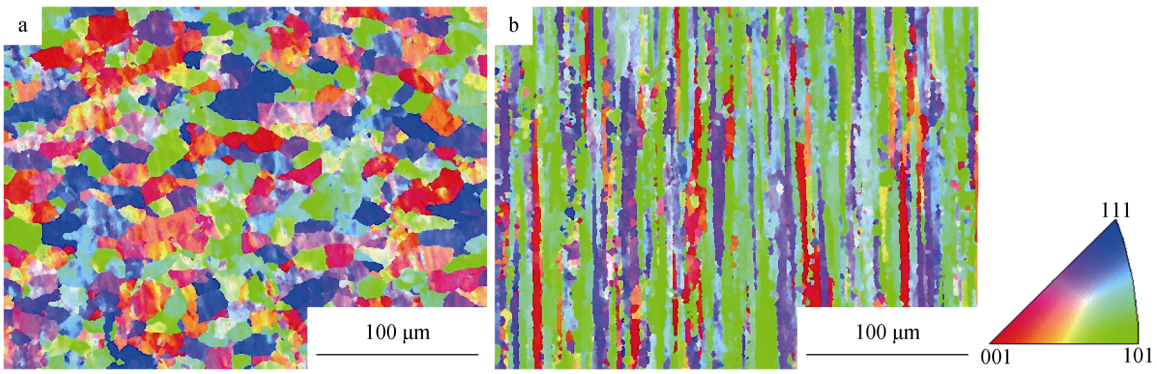

Fig. 4 Orientation images of **a** as-sintered and **b** as-extruded $MgAl_2O_4$ whiskers/6061 Al composites

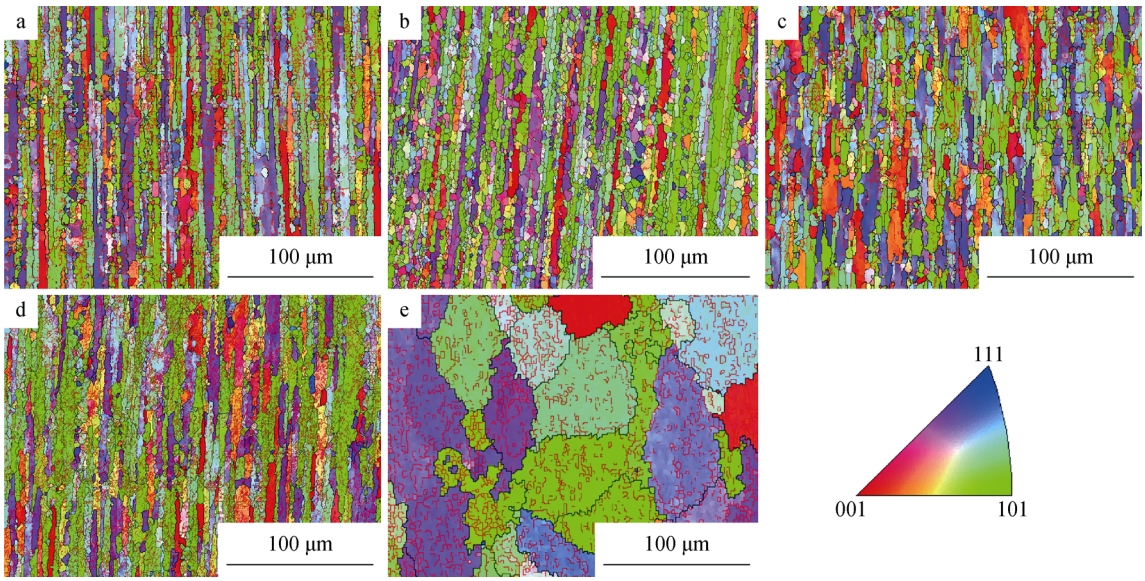

Fig. 5 Orientation images of extruded $MgAl_2O_4$ whiskers/6061 Al composites annealed at different temperatures for 1 h: **a** as-extruded, **b** 530 °C, **c** 580 °C, **d** 600 °C and **e** 630 °C

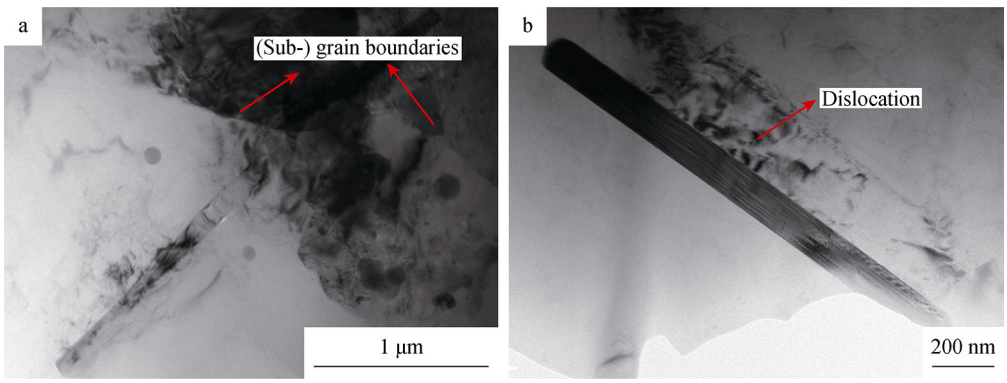

Fig. 6 TEM images showing whiskers distributed at vicinity of **a** (sub-) grain boundaries and **b** dislocation

boundaries (LAGBs, $< 15°$) are colored by red and high-angle grain boundaries (HAGBs, $> 15°$) are colored by black. As mentioned above, a very small amount of fine equiaxed grains have nucleated due to dynamic recrystallization (Fig. 5a). Although fine equiaxed grains exist, most grains are elongated along ED. When specimens were

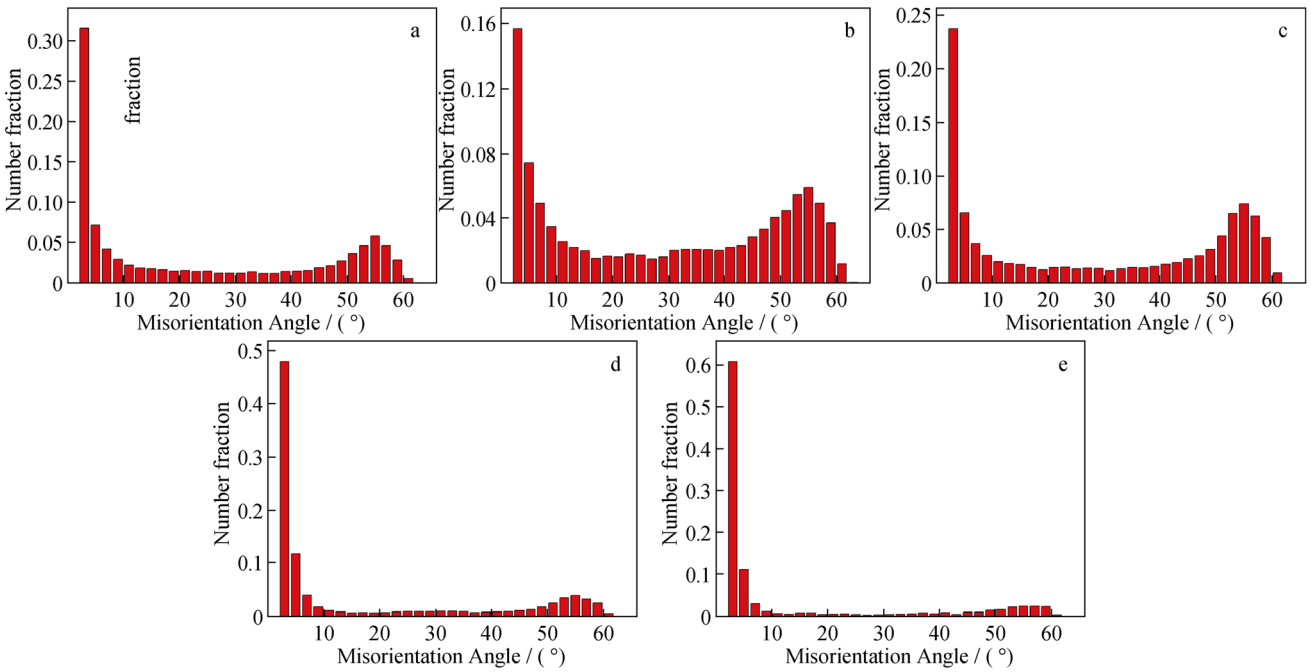

Fig. 7 Misorientation angle distributions of extruded $MgAl_2O_4$ whiskers/6061 Al composites annealed at different temperatures for 1 h: **a** as-extruded, **b** 530 °C, **c** 580 °C, **d** 600 °C and **e** 630 °C

annealed at 530, 580 and 600 °C, the content of equiaxed grains increases and some recrystallized grains start to grow (Fig. 5b–d), compared with as-extruded specimen. Moreover, it is interesting to find that there is no evident difference in recrystallized grains between specimens annealed at 530, 580 and 600 °C. The recrystallization is uncompleted in these specimens. And annealing at 630 °C, the fine recrystallized grains grow into coarse equiaxed grains sharply and no fibrous grain can be observed. This indicates that a complete recrystallization has already occurred.

Compared with the deformed Al–Mg–Si (6xxx series) alloys [13] and SiC/Al composites [27, 29], of which the recrystallization annealing was usually carried out at 500–600 °C, the obtained $MgAl_2O_4$ whiskers reinforced 6061 Al alloy composites show a significant recrystallization resistance. The recrystallization process is retarded since the migration of (sub-) grain boundaries and dislocations is inhibited by the whiskers (Fig. 6). These whiskers were present before recrystallization annealing, which is the essential precondition of Zener pinning [17], and its size is small enough to be regarded as small or closely spaced particles. So according to Zener's pinning equation [30]:

$$Z = k\left(\frac{f\gamma}{r}\right) \tag{6}$$

where r represents the dispersoid radius, k is a scaling factor, f is the content of dispersoid particles (vol%) and γ is the energy of the boundary that the dispersoids pinned. The nano-sized whiskers that located at vicinity of (sub-) grain boundaries and dislocations can offer a strong Zener drag to prevent the movement of dislocations and the migration of grain boundaries, inhibiting the occurrence of recrystallization during annealing.

To characterize the LAGBs and HAGBs, the misorientation angle distribution was investigated (Fig. 7). LAGBs dominate in the as-extruded specimen (Fig. 7a), and the content of LAGBs decreases and that of the HAGBs increases when the specimens were annealed at 530 and 580 °C (Fig. 7b, c). However, when annealed at higher temperatures (600, 630 °C), LAGBs increase continuously even HAGBs hardly can be seen in specimen annealed at 630 °C. It is quite different from the grain boundaries of alloys that have secondary phase dispersions, in which LAGBs decrease and HAGBs increase with annealing temperature increasing [16, 31].

To figure out the reason for this phenomenon, only grain boundaries are shown in Fig. 8, in which LAGBs are colored by red and HAGBs are colored by black. Plenty of LAGBs exist in both deformation sample (Fig. 8a) and annealed samples (Fig. 8b–e). LAGBs do not migrate into HAGBs during recrystallization annealing, but HAGBs decrease because recrystallized grains grow (Fig. 8d, e), resulting in the increase in relative content of LAGBs. And the existence of LAGBs in recrystallized specimens is also caused by the nano-sized whiskers. The whiskers strongly pin LAGBs to prevent their migration (Fig. 6), while migration of HAGBs is not prevented by the whiskers.

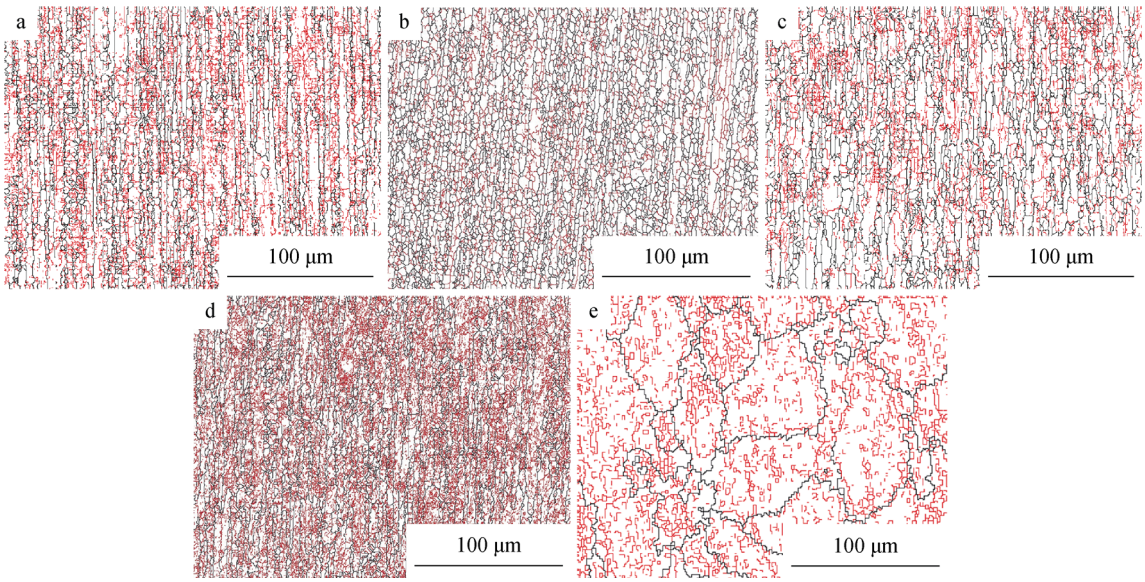

Fig. 8 LAGBs and HAGBs of extruded $MgAl_2O_4$ whiskers/6061 Al composites annealed at different temperatures for 1 h: **a** as-extruded, **b** 530 °C, **c** 580 °C, **d** 600 °C and **e** 630 °C (red lines and black lines indicating LAGBs and HAGBs, respectively)

Thus, relative content of LAGBs increases in specimens annealed at 600 and 630 °C.

3.3 Texture analysis

Texture evolution is important during both the deformation process and recrystallization process since the mechanical properties are related to texture distribution [13]. In general, Goss orientation or other deformation texture components weaken during recrystallization, and cube orientation is usually found to be the dominant recrystallization texture. Since the obtained $MgAl_2O_4$ whiskers reinforced composites show a great recrystallization resistance, it is even necessary to evaluate the texture evolution in annealing process.

Orientation distribution functions (ODFs) of the as-sintered and as-extruded specimens are given in Fig. 9. The textures are formed during hot extrusion (Fig. 9). There is no preferred orientation in as-sintered specimen (Fig. 9a), but deformation textures exist in as-extruded specimen (Figs. 9b, 10a). A strong brass orientation {011} <211> (35° 45° 0°) is found, and an S' component {423} <0–76> (50° 60° 65°) located close to S orientation is found. Moreover, there is an extremely weak cube orientation {001} <100> (0° 0° 0°) in the as-

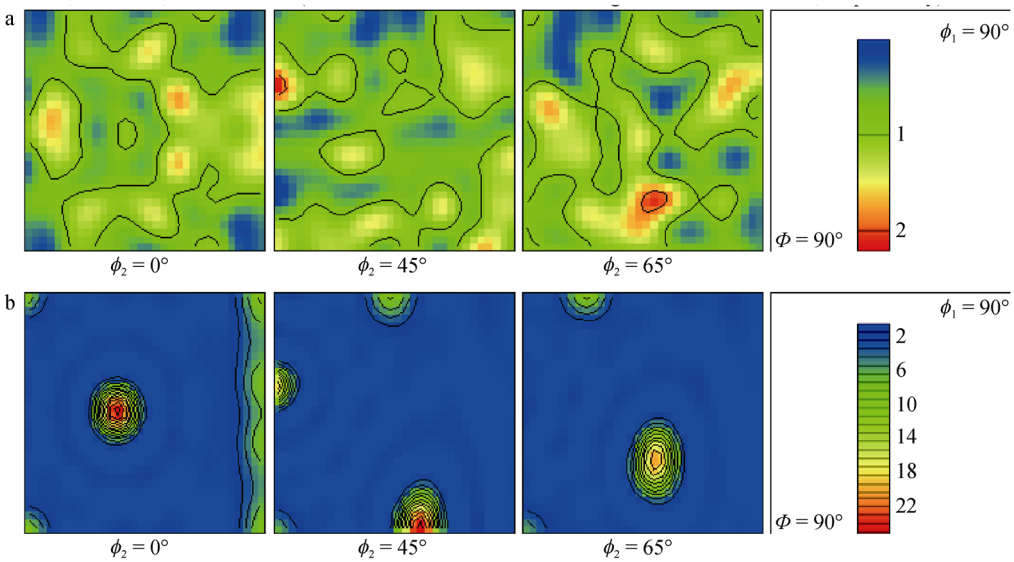

Fig. 9 ODFs with contour line showing texture components of **a** as-sintered and **b** as-extruded $MgAl_2O_4$ whiskers/6061 Al composites

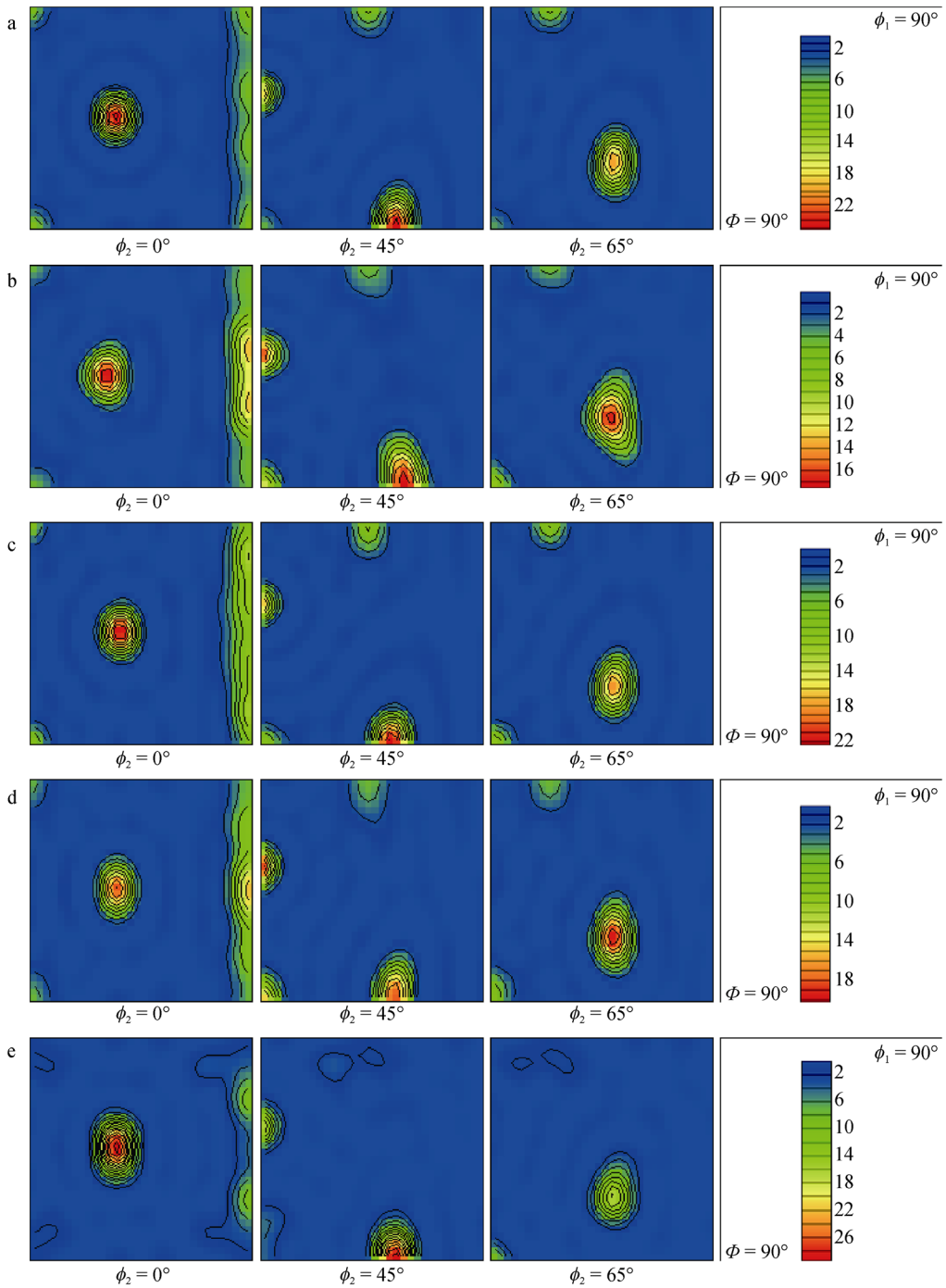

Fig. 10 ODFs of extruded $MgAl_2O_4$ whiskers/6061 Al composites annealed at different temperatures for 1 h: **a** as-extruded, **b** 530 °C, **c** 580 °C, **d** 600 °C and **e** 630 °C

extruded specimen (Figs. 9b, 10a). It indicates that dynamic recrystallization occurs during the hot extrusion, which agrees with the result of microstructural observation (Figs. 4b, 5a). The same texture components are also found in annealed specimens (Fig. 10b–e), with little differences in location and intensity that could be neglected. The result is consistent with the microstructure of specimens annealed at 530, 580 and 600 °C (Fig. 5b–d) since recrystallization is retarded by the whiskers.

It is worth mentioning that even in completely recrystallized specimen the deformation textures are still retained and no recrystallization texture is detected (Figs. 5e, 10e).

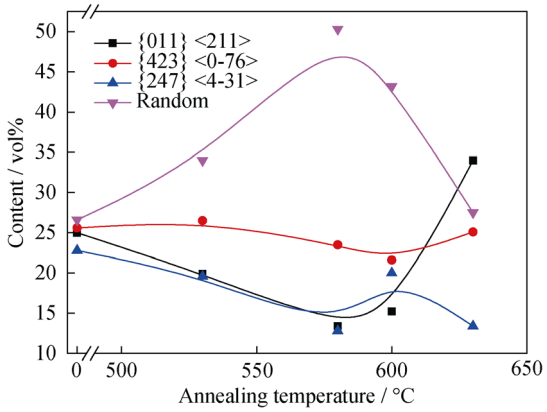

Fig. 11 Content of major texture components in $MgAl_2O_4$ whiskers/6061 Al composites with annealing temperature

This phenomenon is sometimes found in the recrystallization textures of alloys containing small non-deformable particles which are present before deformation [17]. It can be explained by the theory first proposed in 1949 [17] that the new grains do not 'nucleate' as totally new grains through the atom-by-atom construction. These new grains grow from small regions, recovered sub-grains or cells, which are already present in the deformed microstructure. It results in the orientation of new grain arises from the same orientation present in the deformed state, and thus the deformation textures remain and no recrystallization texture appears.

Figure 11 shows the content of three major texture components. Beside the two deformation textures mentioned above, another texture is found as {247} <4–31> (20° 35° 25°), and its content decreases overall with the annealing temperature increasing. The brass component first decreases and then increases, reaching the bottom at about 580 °C, and its content of completely recrystallized specimen (annealed at 630 °C) is even higher than that of as-extruded specimen. Meanwhile, S' component fluctuates slightly with annealing temperature, but almost remains the same as non-annealed. In addition, the total content of these three major texture components first decreases then increases and reaches the minimum at about 580 °C.

3.4 Mechanical properties

Table 1 lists the tensile and hardness test results of the as-extruded specimen and the samples annealed at different temperatures. The ultimate tensile strength (UTS) of as-extruded specimen is 285 MPa and the elongation to failure is 9.4%. The UTS declines gradually with the annealing temperature increasing up to 600 °C. The elongation presents slight difference in the specimens annealed at 530, 580 and 600 °C, but a sharp decrease can be found for the specimen annealed at 630 °C. The similar trend exists for hardness. Fracture appearances of the specimens are shown in Fig. 11. Obvious deep ductile dimples are distributed on the fracture surface of as-extruded specimen (Fig. 12a), and the whiskers are found in dimples (Fig. 12b), indicating that the load is effectively transferred to the whiskers. The cross section of whiskers can be observed since most of the whiskers lay along ED (Fig. 3a, b). There are also plenty of dimples in specimens annealed at 530 and 580 °C. However, in specimens annealed at 600 and 630 °C, few ductile dimples can be observed and some deep pores appear due to the partly melting of the matrix at high annealing temperature, leading to the poor toughness especially in the specimen annealed at 630 °C.

Table 1 Mechanical properties of as-extruded sample and samples annealed at different temperatures

Samples	UTS/MPa	Elongation/%	Hardness (HV)
As-extruded	285	9.4	69
Annealed at 530 °C	246	9.9	61
Annealed at 580 °C	239	10.4	60
Annealed at 600 °C	234	9.3	59
Annealed at 630 °C	218	4.6	52

The mechanical properties of the AMCs depend on the reinforcement, the microstructure of the matrix and a strong reinforcement–matrix interface. The as-extruded composite exhibits the highest strength and hardness among all the examined specimens, which can be attributed to the orientation-aligned reinforcement and the grain refinement after the partly dynamic recrystallization. UTS and hardness of the specimens annealed at 530, 580 and 600 °C are lower than those of as-extruded sample due to the growth of some recrystallized grains, which is consistent with the microstructural evolution shown in Fig. 8. The strength and hardness of these three samples show a slight decrease with the annealing temperature increasing due to the contribution of uniformly distributed whiskers. However, the grains of specimen annealed at 630 °C grow equiaxed and extremely coarse, resulting in the decline in strength and hardness. Even worse, ductile dimples can hardly be found in the specimen annealed at 630 °C and pores are much larger and deeper than those of specimen annealed at 600 °C, so micro-cracks tend to form when subjecting to tensile stress, resulting in the poor elongation to failure. The microstructure stability at high temperatures indicates that the obtained AMCs have potential application at elevated temperatures.

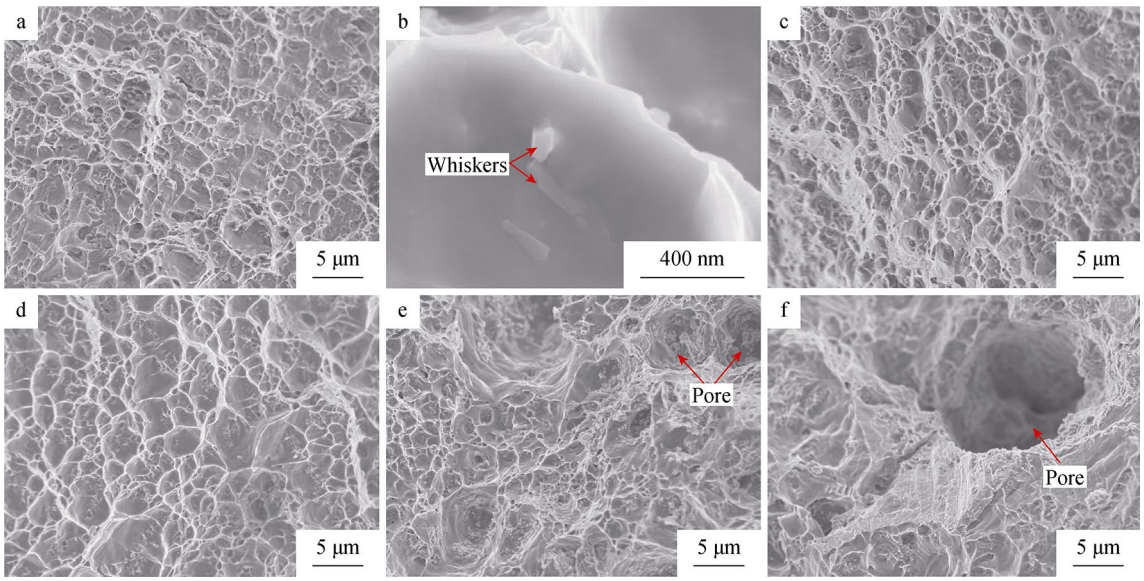

Fig. 12 SEM images for fracture morphologies of extruded $MgAl_2O_4$ whiskers/6061 Al composites annealed at different temperatures for 1 h: **a, b** as-extruded, **c** 530 °C, **d** 580 °C, **e** 600 °C and **f** 630 °C

4 Conclusions

Nano-sized $MgAl_2O_4$ spinel whiskers were in situ synthesized in 6061 Al alloys during sintering, and the diameter of whiskers ranges from 30 to 100 nm with the aspect ratio ranging from 10 to 30. The whiskers lay along ED after hot extrusion and strongly bond with the matrix through a clean and smooth interface. The whiskers located at vicinity of grain boundaries, sub-grain boundaries and dislocations may offer great Zener drag to them, inhibiting their migration during annealing, and thus the recrystallization is retarded. The microstructure of annealed specimens shows slight difference till the recrystallization completed, when the grains grow coarse and HAGBs decrease sharply with LAGBs retaining. Deformation textures are Brass orientation and a texture closed to S orientation, and they remain during recrystallization. The change of mechanical properties agrees with the microstructural evolution. Both UTS and Vickers hardness drop slightly when annealed at 530, 580 and 600 °C and quickly decline at 630 °C. When annealed at temperatures higher than 630 °C, part of matrix melts, resulting in the poor elongation in specimen.

Acknowledgements This work was financially supported by the National Natural Science Foundation of China (No. 51571147).

References

[1] Bakshi SR, Lahiri D, Agarwal A. Carbon nanotube reinforced metal matrix composites—a review. Int Mater Rev. 2013;55(1):41.

[2] Prater T. Friction stir welding of metal matrix composites for use in aerospace structures. Acta Astronaut. 2014;93:366.

[3] Tjong SC, Ma ZY. Microstructural and mechanical characteristics of in situ metal matrix composites. Mater Sci Eng R. 2000;29(3):49.

[4] He C, Zhao N, Shi C, Du X, Li J, Li H, Cui Q. An approach to obtaining homogeneously dispersed carbon nanotubes in Al powders for preparing reinforced Al-matrix composites. Adv Mater. 2007;19(8):1128.

[5] Guo C, Zou T, Shi C, Yang X, Zhao N, Liu E, He C. Compressive properties and energy absorption of aluminum composite foams reinforced by in situ generated $MgAl_2O_4$ whiskers. Mater Sci Eng A. 2015;645:1.

[6] Yu Z, Zhao N, Liu E, Shi C, Du X, Wang J. Fabrication of aluminum matrix composites with enhanced mechanical properties reinforced by in situ generated $MgAl_2O_4$ whiskers. Compos Part A Appl Sci Manuf. 2012;43(4):631.

[7] Zhou Y, Zhao N, Shi C, Liu E, Du X, He C. In-situ processing and aging behaviors of $MgAl_2O_4$ spinel whisker reinforced 6061Al composite. Mater Sci Eng A. 2014;598:114.

[8] Xing L, Zhang Y, Shi C, Zhou Y, Zhao N, Liu E, He C. In-situ synthesis of $MgAl_2O_4$ nanowhiskers reinforced 6061 aluminum alloy composites by reaction hot pressing. Mater Sci Eng A. 2014;617:235.

[9] Wei H, Li Z, Xiong DB, Tan Z, Fan G, Qin Z, Zhang D. Towards strong and stiff carbon nanotube-reinforced high--strength aluminum alloy composites through a microlaminated architecture design. Scr Mater. 2014;75:30.

[10] Chen CG, Luo J, Guo ZM, Yang WW, Chen J. Microstructural evolution and mechanical properties of in situ TiB_2/Al composites under high-intensity ultrasound. Rare Met. 2015;34(3):168.

[11] Sreekumar VM, Pillai RM, Pai BC, Chakraborty M. A study on the thermodynamics of in situ $MgAl_2O_4$/Al MMC formation using amorphous silica sources. J Mater Process Technol. 2007;192–193:588.

[12] Mao CH, Sun XD, Liang QS, Yang J, Du J. Interfacial reaction process of the hot-pressed WC/2024Al composite. Rare Met. 2013;32(4):397.

[13] Engler O, Hirsch J. Texture control by thermomechanical processing of AA6xxx Al–Mg–Si sheet alloys for automotive applications—a review. Mater Sci Eng A. 2002;336(1–2):249.
[14] Huang K, Li YJ, Marthinsen K. Factors affecting the strength of P{011} <566>-texture after annealing of a cold-rolled Al–Mn–Fe–Si alloy. J Mater Sci. 2015;50(14):5091.
[15] Deng Y, Zhang Y, Wan L, Zhang X. Effects of thermomechanical processing on production of Al–Zn–Mg–Cu alloy plate. Mater Sci Eng A. 2012;554:33.
[16] Deng Y, Xu G, Yin Z, Lei X, Huang J. Effects of Sc and Zr microalloying additions on the recrystallization texture and mechanism of Al–Zn–Mg alloys. J Alloys Compd. 2013;580:412.
[17] Doherty RD, Hughes DA, Humphreys FJ, Jonas JJ, Juul Jensen D, Kassner ME, King WE, McNelley TR, McQueen HJ, Rollett AD. Current issues in recrystallization: a review. Mater Sci Eng A. 1997;238(2):219.
[18] Duan YL, Xu GF, Peng XY, Deng Y, Li Z, Yin ZM. Effect of Sc and Zr additions on grain stability and superplasticity of the simple thermal–mechanical processed Al–Zn–Mg alloy sheet. Mater Sci Eng A. 2015;648:80.
[19] Nikulin I, Kipelova A, Malopheyev S, Kaibyshev R. Effect of second phase particles on grain refinement during equal-channel angular pressing of an Al–Mg–Mn alloy. Acta Mater. 2012;60(2):487.
[20] Li H, Gao Z, Yin H, Jiang H, Su X, Bin J. Effects of Er and Zr additions on precipitation and recrystallization of pure aluminum. Scr Mater. 2013;68(1):59.
[21] Deng Y, Peng B, Xu G, Pan Q, Yin Z, Ye R, Wang Y, Lu L. Effects of Sc and Zr on mechanical property and microstructure of tungsten inert gas and friction stir welded aerospace high strength Al–Zn–Mg alloys. Mater Sci Eng A. 2015;639:500.
[22] Jiang X, Galano M, Audebert F. Extrusion textures in Al, 6061 alloy and 6061/SiC_p nanocomposites. Mater Charact. 2014;88:111.
[23] Kumar P, Kawasaki M, Langdon TG. Review: overcoming the paradox of strength and ductility in ultrafine-grained materials at low temperatures. J Mater Sci. 2015;51(1):7.
[24] Huang K, Logé RE, Marthinsen K. On the sluggish recrystallization of a cold-rolled Al–Mn–Fe–Si alloy. J Mater Sci. 2015;51(3):1632.
[25] Yan LZ, Zhang YA, Xiong BQ, Li XW, Li ZH, Liu HW, Huang SH, Zhao G. Mechanical properties, microstructure and surface quality of Al-1.2Mg-0.6Si-0.2Cu alloy after solution heat treatment. Rare Met. 2017;36(7):550.
[26] Zhang JX, Zhang KL, Liu YT, Zhong L. Microstructure and texture evolution of 6016 aluminum alloy during hot compressing deformation. Rare Met. 2014;33(4):404.
[27] Zhang WL, Gu MY, Wang DZ, Yao ZK. Rolling and annealing textures of a SiC_w/Al composite. Mater Lett. 2004;58(27–28):3414.
[28] Soltani S, Azari Khosroshahi R, Taherzadeh Mousavian R, Jiang ZY, Fadavi Boostani A, Brabazon D. Stir casting process for manufacture of Al–SiC composites. Rare Met. 2017;36(7):581.
[29] Poudens A, Bacroix B. Recrystallization textures in Al–SiC metal matrix composites. Scr Mater. 1996;34(6):847.
[30] Wu LM, Wang WH, Hsu YF, Trong S. Effects of homogenization treatment on recrystallization behavior and dispersoid distribution in an Al–Zn–Mg–Sc–Zr alloy. J Alloys Compd. 2008;456(1–2):163.
[31] Liu J, Yao P, Zhao N, Shi C, Li H, Li X, Xi D, Yang S. Effect of minor Sc and Zr on recrystallization behavior and mechanical properties of novel Al–Zn–Mg–Cu alloys. J Alloys Compd. 2016;657:717.